

Influence of Fe³⁺ ions on the crystallographic, optical and electrochemical performance of ZnS quantum dots

P Sakthivel^{1*} , A Krishnamoorthy^{2*} and I Devadoss²

¹Department of Physics, Centre for Materials Science, Science and Humanities, Faculty of Engineering, Karpagam Academy of Higher Education, Coimbatore, Tamil Nadu 641 021, India

²PG and Research Department of Physics, Bishop Heber College (Affiliated to Bharathidasan University), Tiruchirappalli, Tamil Nadu 620 017, India

Received: 14 February 2023 / Accepted: 25 July 2023 / Published online: 21 August 2023

Abstract: Analysing the impact of Fe³⁺ dopant on the structural, morphological, optical, and electrochemical characteristics of ZnS quantum dots is the goal of the current work. The Fe³⁺ ions doped ZnS QDs were prepared using the coprecipitation technique, and the Fe³⁺ doping percentage was tuned to 0,1,3 and 5 at.%. The crystalline structure and phase information have been verified through X-ray diffraction. The crystallite size of the ZnS QDs reduces gradually as a function of Fe³⁺ doping concentration. The size of a crystallite was calculated to be about 2 nm. The structural and morphological validation of Fe³⁺-doped ZnS QDs was supported by the TEM and SEM data. To ensure the presence of the elements, the stoichiometry ratio and molecular vibrations were determined by EDAX and FT-IR analyses. A UV–vis optical study revealed that a maximum transmittance was received in the visible region for Fe³⁺ (5 at.%) doped ZnS quantum dots. Initial substitution of Fe³⁺ ions led to a blue shift in the band gap; further doping exhibited a red shift. The intensity of PL emission in the blue region is remarkably reduced due to the doping ions. The electrochemical study revealed that Fe³⁺ (5 at.%) doped ZnS quantum dots possess a better electrical response. The specific capacitance was enhanced due to Fe³⁺ ion doping.

Keywords: ZnS; Fe³⁺; Band gap; Photoluminescence; Transmittance

1. Introduction

Recently, semiconductor quantum dots (SQDs) have played a vital role in fabricating optical, optoelectronic and luminescent devices [1]. SQDs are nanomaterials with zero dimensions, and the particles' sizes range from 1 to 10 nm. Due to their state-of-the-art capabilities, SQDs are widely used in a variety of cutting-edge applications, including computing, communications, solid-state lighting, lasers, quantum optics, photovoltaics, luminescence, biology, bioimaging and biosensing, and biomedical applications [2–5].

The materials used for tailoring the optical band gap for a broad range [6] are II–VI semiconductors. Solar cells, wearable electronics, photodetectors, biosensors, blue LEDs, and spintronics are just a few of the devices that use

II–VI semiconductors. Paul O'Brien et al. discussed current advancements in II–VI and III–VI semiconductors as well as their uses in solar cells [7–12].

Researchers are more interested in ZnS in the II–VI semiconductor family because of its excellent outcomes and applicability in a variety of fields [13, 14]. One of the earliest identified semiconductors, ZnS, has two distinct structures, the cubic phase and the hexagonal phase. At ambient temperature, ZnS offers a significant exciton binding energy of 39 meV, a broad direct band gap (3.6 eV), and support for n and p-doping [15]. ZnS shows polymorphism because there are two primary crystalline forms that can be identified, the most stable of which is zincblende (ZB) below 1290 K and the high-temperature, synthetically feasible allotrope with wurtzite (WZ) symmetry. From visible wavelengths to just over 12 μm, ZnS exhibits a very high transmittance, making it transparent across an exceptionally wide energy range [16].

ZnS doping of transition metals improves the morphological, structural, optical, electrical, and magnetic

*Corresponding author, E-mail: sakthi1807@gmail.com; krishnamoorthydomala@gmail.com

properties of the host materials [17]. ZnS-based nanostructures were key in light-emitting and photovoltaic applications [18]. ZnS Quantum Dots (QDs) exhibit excellent adaptability for preceding the doping process. Transition metal doping, or co-doping, has been found to have an impact on the physical properties of semiconducting nanoparticles or nanocomposites, including luminescence, photocatalytic activity, and electrochemical properties. It has been proposed that transition metal-doped ZnS nanoparticles could be used to create lighting devices [19].

When Fe was doped with ZnS nanoparticles, photoluminescence efficiency enhancement was observed in an earlier study [20]. Fe-doped ZnS QDs produced a visible light emission used for white light emitting technologies [21]. Fe-doped ZnS lattices exhibited their effective light response in the visible-light region [22]. Room temperature ferromagnetism was observed on Fe-doped ZnS thin films, leading to spintronics applications [23]. Smaller crystallite size and band gap tailoring for a wide range were tuned through Fe and Co doping on ZnS nanoparticles [24].

Ni, Fe doped ZnS nanopowders' optical and magnetic characteristics were discussed [25]. Fe-doped ZnS was the subject of a theoretical investigation, and the existence of half-metallic ferromagnetism was proven [26]. Fe-doped ZnS QDs received an increase in fluorescence capacity, which was analyzed through a DFT approach [27]. The role of Fe ions in influencing magnetic properties has been demonstrated in many research studies. The present discussion is about the effect of Fe ions on the structural, morphological, elemental, optical, and electrochemical properties of ZnS. Though some results are related to the investigations of the structural, optical, and magnetic properties of Fe-doped ZnS QDs, the optimization of crystallite size and properties still requires more work. Moreover, the electrochemical properties of Fe-doped ZnS QDs are scanty in the literature. Even though there are many methods available for the synthesis of QDs, the co-precipitation method is employed for this present synthesis since it has advantages like ease of mass production, cost-effectiveness and simplicity [28]. Here, the Fe³⁺-doped ZnS QDs were synthesized using the co-precipitation method without using any capping agent and their structural, morphological, elemental, optical, photoluminescent and electrochemical properties were analyzed.

2. Experimental details

2.1. Materials

Zinc acetate ($\text{Zn}(\text{CH}_3\text{COO})_2 \cdot 2\text{H}_2\text{O}$), and sodium sulfide (Na_2S) were used as precursor materials. Ferric chloride

(Fe_3Cl_3) was taken as a dopant. All the chemicals belong to the AR grade with 99.5% purity and were purchased from M/s Merck. The De-ionized (DI) water is a solvent to dissolve the chemicals. Ammonia solution (NH_4OH) was used to stabilize the pH value.

2.2. Preparation of Fe-doped ZnS QDs

The co-precipitation technique was used to create both undoped and Fe-doped ZnS QDs. According to the desired stoichiometry ratio, the chemicals were taken to prepare the separate chemical solutions, using de-ionized ultra-pure distilled water as solvent. Initially, zinc acetate and sodium sulfide were weighed and dissolved in de-ionized water in separate beakers using magnetic stirring until completely dissolved. Then, based on the doping composition ratio, the ferric chloride was dissolved in DI water and added dropwise to the ZnS solution. The pH value was set to 9 using an ammonia solution. The chemicals were well dissolved using a magnetic stirrer with a stirring rate of 1000 rpm for 5 h. Once the chemical reaction was complete, the precipitate fell to the flask's bottom and settled there. These precipitates were taken out and dried using a vacuum oven (Make: Wee Scientific) for 8 h at 65 °C. The dried samples were collected and ground finely using agate mortar. The same procedure was repeated to prepare the ZnS: Fe with different compositions (0, 1,3 and 5 at.%).

2.3. Characterization techniques

An X-ray diffractometer (Model: Rigaku Make: C/max-2500) was used to record XRD diffractograms in order to examine the structural data and phase purity.

A transmission electron microscope (Make: Philips, model: CM 200, operating voltage range: 20–200 kV) was used to get the TEM data. Energy dispersive X-ray (EDAX) and scanning electron microscopy (SEM) were used, respectively, for elemental and surface morphological investigations. The SEM (Make: JEOLJSM, model: 6390) was used for the aforesaid study. The molecular vibrations were explored using a Fourier Transform Infrared (FT-IR) spectrometer (model: Perkin Elmer, make: Spectrum RXI). A UV-Vis spectrometer (Model: Lamda 35, make: Perkin Elmer) was used to record the UV-Vis spectral features. The photoluminescence spectra of ZnS and Fe-doped ZnS QDs were taken using a PL spectrometer (model: F-2500, make: Hitachi). To perform CV analysis, a cyclic voltameter was used (Model: VersaSTAT MC electrochemical system, Make: Princeton Applied Research, USA).

3. Results and discussion

3.1. Structural, morphological and elemental analysis

Figure 1 illustrates the X-ray diffractograms of undoped ZnS and Fe³⁺-doped ZnS QDs ($2\theta = 10^\circ$ to 80°). The observed predominant peaks confirmed that the samples have a cubic zinc blend structure without forming mixed phases. The high-intense peak position was slightly shifted to a larger 2θ angle side, which confirmed the dopant has substituted well into the host lattice. The JCPDS file number 05-0566 is indexed to the primary peak position and confirms the cubic phase [29]. The crystallite size of the ZnS and Fe³⁺ incorporated ZnS QDs was calculated using Debye's Scherrers' formula [30]

$$\text{Crystallite size } (D) = \frac{0.9\lambda}{\beta \cos \theta} \quad (1)$$

where θ denotes the Bragg diffraction angle, β denotes the Full-width half-wave at maximum, and λ is the wavelength of the utilized X-ray.

The peak intensity was reduced gradually with the increase in Fe³⁺ concentration. The peak position (2θ) value is shifted to the low-frequency side due to the addition of Fe³⁺ dopant in the ZnS host lattice. This change in peak position ensured the effective doping of Fe³⁺ ions. The gradual decrement in primary peak intensity evidences the decrease in particle size. As a result, the crystallite size of Fe³⁺ ions-doped ZnS QDs was reduced gradually. This size tuning is endorsed by the variation of the ionic radius of Zn²⁺ (0.74 Å) and Fe³⁺ 0.63 Å. This variation reduced the overall particle size [31]. The discovered lattice parameter for the current inquiry was the same as that published before (ICSD 651457, 5.4093 Å).

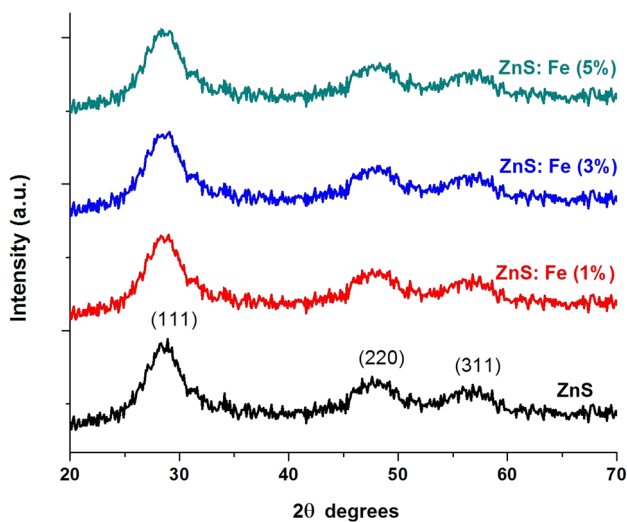


Fig. 1 XRD spectrographs of ZnS and Fe³⁺-doped ZnS QDs

Crystallite size is gradually decreased for every increase in Fe³⁺ doping ratio. The dislocation density and microstrain increased due to the increase of the Fe³⁺ doping ratio. The lattice parameter, crystallite size, FWHM value, 2θ position, dislocation density and micro-strain are listed in Table 1.

Due to their displacement from their optimum places in the structure, the addition of foreign particles may cause dislocations in the planes. Consequently, dislocation densities for all of the samples were computed using Eq. (2) to understand the impact of the changes [17].

$$\text{Dislocation density } (\delta) = \frac{1}{D^2} \quad (2)$$

The rise in dislocation density confirms the formation of the quantum structures. P. Kumari et al. discovered a comparable rise in dislocation density in Ce-doped ZnS structures. [32]. The microstrain produced in the crystal structure was calculated using the following relations [33].

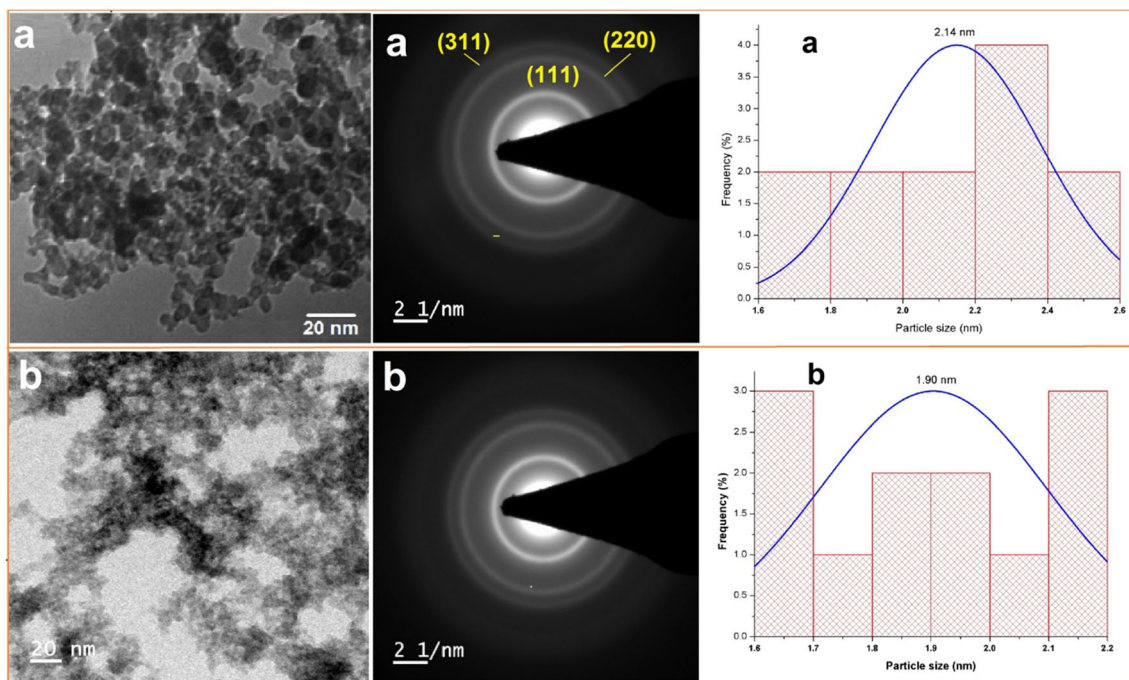
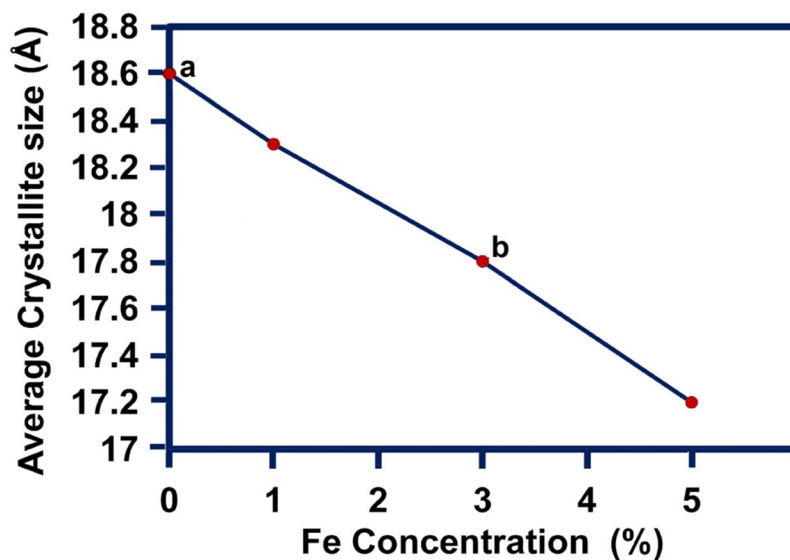
$$\text{Micro - Strain } (\varepsilon) = \frac{\beta}{4 \tan \theta} \quad (3)$$

As the amounts of Fe³⁺ doping rose, the microstrain was steadily rised. The change in crystallite size and ionic radii provides evidence of the rise in microstrain. The particle size of the ZnS: Fe³⁺ QDs vs Fe³⁺ doping concentration was plotted in Fig. 2. The role of Fe³⁺ ion doping reduces the overall crystallite size of the ZnS QDs. The TEM pictures, along with histogram analysis and their SAED patterns of undoped ZnS QDs, and Fe³⁺ doped (3 at. wt%) ZnS QDs were presented in Fig. 2. These pictures revealed that small-sized spherical-shaped particles were present, and the incorporation of Fe³⁺ reduced the size of the particles. The size estimation through histograms was performed using the Image J tool. The decrease in particle size due to the doping of Fe³⁺ ions is also confirmed by the results obtained from TEM. The SAED patterns confirmed the planes that we obtained through XRD studies {(111) (220) (311)}. The diffraction ring indexed with the (111) plane showed high brightness and conformity with XRD peaks.

SEM has been utilized to investigate the surface and morphological information of samples. Figure 3a-c discloses the surface morphology of Fe³⁺ (0 at.%, 1 at.% and 3 at.%) doped ZnS nanoparticles. The particles present on the surface induced the smoothing as a function of the doping concentration of Fe³⁺ ions. The small-sized Fe³⁺ ions occupied the interspaces between Zn²⁺ lattices. The EDAX spectrum of Fe³⁺-doped ZnS nanoparticles is also given in Fig. 3a-c, corresponding to the SEM images. All the elements were present in the photograph as per the expected ratio. The presence of elements and their Atomic weight percentage are given in Table 2.

Table 1 The peak position, FWHM, Lattice parameter and Crystallite size of Fe³⁺ doped ZnS QDs

Quantum dots	Peak position 2θ (°)	FWHM (°)	d ₍₁₁₁₎ (Å)	Lattice parameter a [Å]	Crystallite size D (Å)	Dislocation Density (δ) × 10 ¹⁵ m ⁻²	Micro strain (ε) × 10 ⁻³
ZnS	28.56	4.44	3.125	5.411	18.46	293.35	76.11
Zn _{0.99} Fe _{0.01} S	28.65	4.62	3.113	5.398	17.74	317.49	78.94
Zn _{0.97} Fe _{0.03} S	28.71	4.73	3.108	5.378	17.33	322.71	80.64
Zn _{0.95} Fe _{0.05} S	28.78	4.79	3.102	5.367	17.12	341.09	81.46

**Fig. 2** Fe doping concentration Vs Average Crystallite size & TEM photograph, SAED pattern and Histogram of (a) Undoped ZnS (b) Fe³⁺ doped (3 at. wt%) ZnS QDs

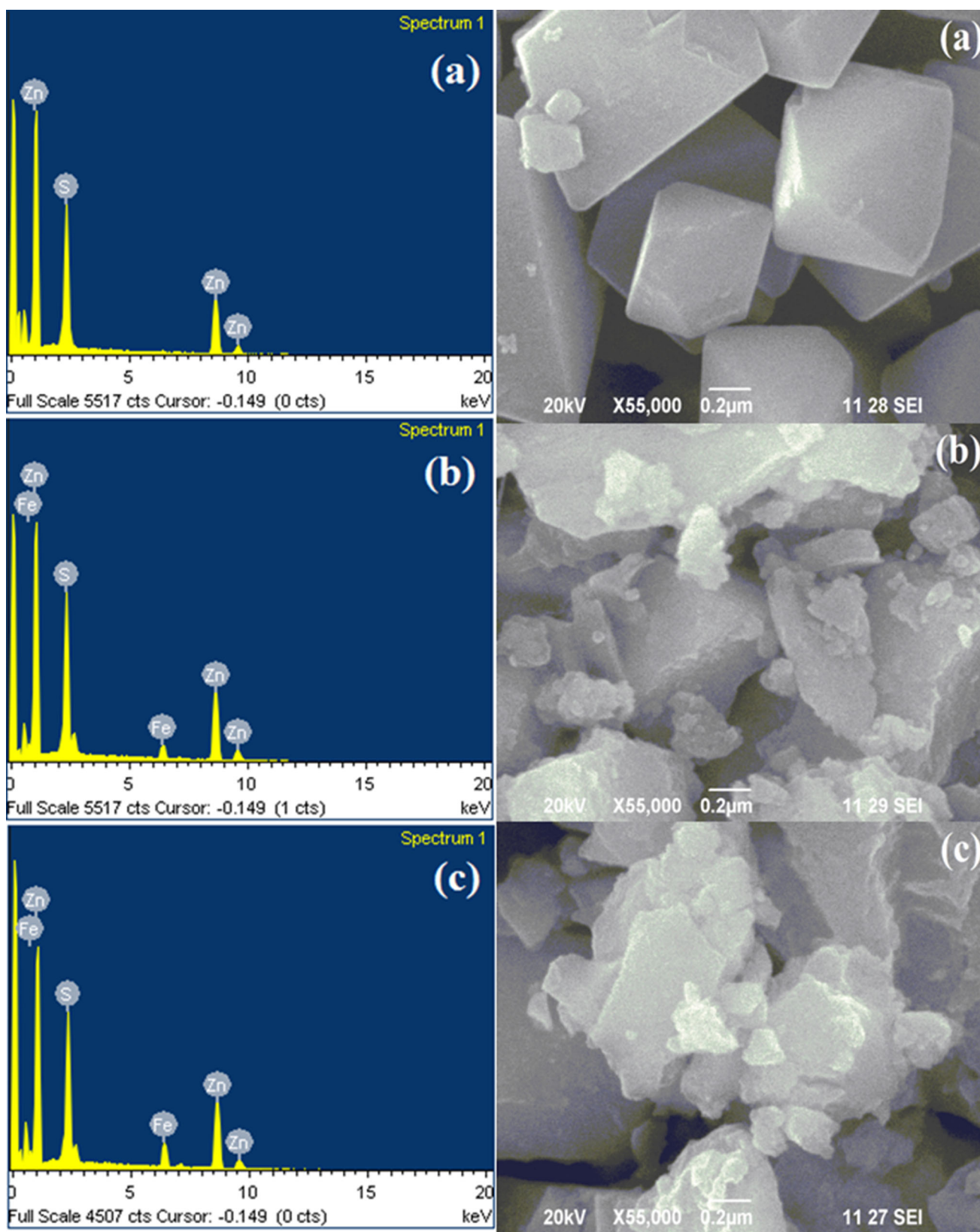


Fig. 3 EDAX and SEM Photographs of (a) = Fe^{3+} (0%), (b) = Fe^{3+} (1%), (c) = Fe^{3+} (3%) – doped ZnS QDs

Use of Taucs' formula obtains the optical band gap value [37]

$$\alpha hv = A(hv - E_g)^n \quad (5)$$

where A is a constant, E_g is an energy gap, and n represents the type of transition, where hv is the photon energy. For authorised direct, allowed indirect, 3/2 forbidden direct, and 3 forbidden indirect transitions, the values of n are 1/2, 2, and 3/2, respectively. In Fig. 7, the Tauc's plot for the current samples is displayed. For initial doping, the band gap was slightly blue-shifted (It is shifted from 4.096 eV to 4.11 eV) and a further increase in doping concentration reduces the band gap value (4.11 eV to 4.095 eV). The increase in band gap is ascribed to the quantum confinement effect. The energy gap reduction is observed in Fe-doped ZnS [23]. The extension of the energy gap due to Fe-doping may be attributed to the size quantization effect [38]. A small red shift for further doping of Fe³⁺ ions is due to the larger addition of Fe and leads to a direct energy transfer from the excited states to the 3d levels of Fe³⁺ ions [39]. But these variations of particle size did not produce a huge change in the Band gap of ZnS QDs.

3.4. Photoluminescence

The PL spectra of undoped and Fe³⁺-doped ZnS QDs are illustrated in Fig. 8. The intensity corresponding to blue-centered white emission was high in pure ZnS QDs and was suppressed due to the incorporation of Fe³⁺ ions. A small emission peak received in the UV region disappeared in Fe³⁺-doped ZnS QDs. A similar quenching of emission intensity on ZnS QDs due to Fe³⁺ ions was observed in an earlier study [40]. The blue-green emission arising in ZnS QDs is due to the quantization of the band gap. The defect states played a major role in this emission, where electrons create a trap in the conduction band. A non-radiative transition between the holes in the valence band and electrons in the conduction band converted into a radiative

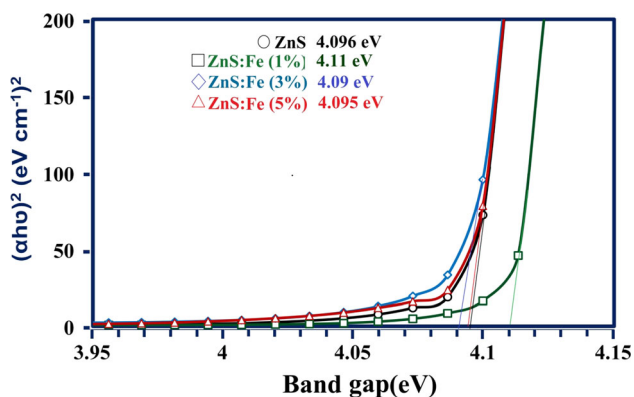


Fig. 7 Energy gap values of ZnS and Fe³⁺-doped ZnS QDs

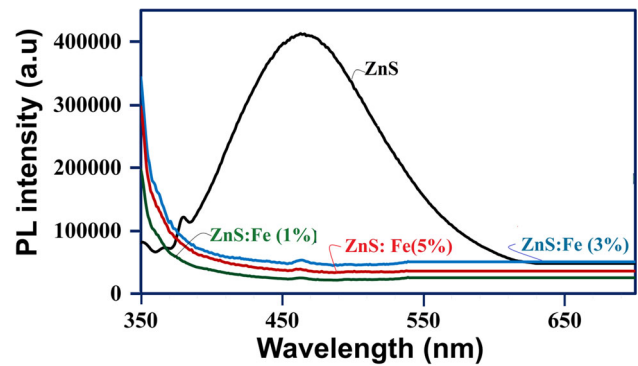


Fig. 8 PL spectra of undoped ZnS and Fe³⁺-doped ZnS QDs

transition [41]. Figure 9 illustrates the CIE chromaticity diagram of Fe³⁺-doped ZnS QDs. It indicates strong white and blue colour emissions.

3.5. Electrochemical analysis

Cyclic Voltammetry (CV) is a basic and essential tool to investigate the current development of an electrochemical cell. Figure 10a–d illustrates the cyclic voltammograms of Fe³⁺-doped ZnS QDs. In the current study, the cathodic current density (J_{pc}) and anodic current density (J_{pa}) were measured [42]. The high current peak value (J_{pc}) was obtained for Fe³⁺ (5 at.%) doped in ZnS QDs. The value of ΔE_p is calculated by the relation given below. Where ΔE_p is denoted as the peak-to-peak separation value. Here, undoped ZnS QDs gave a low ΔE_p value [43].

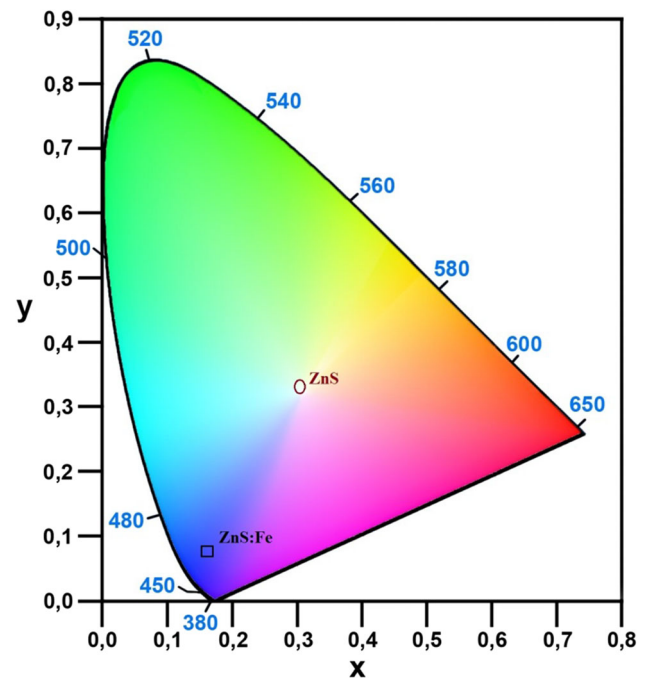
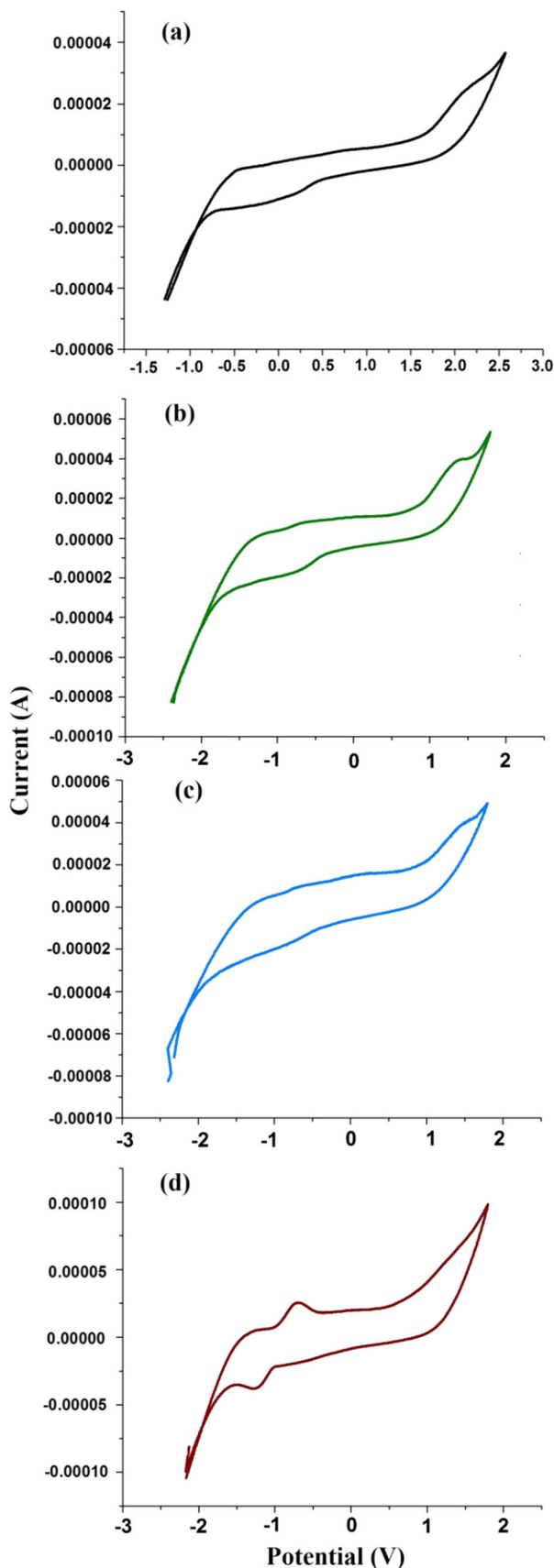


Fig. 9 CIE Chromaticity diagram of ZnS and Fe³⁺-doped ZnS QDs



◀**Fig. 10** Cyclic Voltammetry study of ZnS and Fe³⁺-doped ZnS QDs. (a) = Fe³⁺ (0%), (b) = Fe³⁺ (1%), (c) = Fe³⁺ (3%) and (d) = Fe³⁺ (5%)

$$\Delta E_p = E_{pc} - E_{pa} \quad (6)$$

The cathode peak current (I_{pc}) and anode peak current (I_{pa}) are increased when the Fe³⁺ doping ratio is increased. This response confirmed the increase in ionic conductivity. Among the responses received from the various concentrations of Fe³⁺ ions with ZnS QDs, Fe³⁺ 5 at.% doped samples exhibited better electrical behavior. The increase in ΔEP value due to Fe³⁺ ion doping ensured that the samples exhibited good electrochemical stability, which led to a redox couple. The increase in peak broadness and surface area due to the increase of Fe³⁺ ions in ZnS QDs confirmed the increase in specific capacitance.

The potential vs. Time responses were recorded for galvanostatic charge–discharge cycling and plotted in Fig. 11. It shows a ramp waveform. Using current density and potential, a specific capacitance value was found [44]. The scan rate, area, potential window, and specific capacitance were listed in Table 3. Fe³⁺ ions enhanced the specific capacitance value of ZnS QDs. It is declined only for 5 at.% Fe³⁺-doped ZnS QDs. The increasing trend of specific capacitance due to Fe³⁺ ion doping with ZnS QDs is depicted in Fig. 12.

4. Conclusions

In summary, the Fe³⁺ ion incorporated ZnS QDs have been prepared using the co-precipitation method. X-ray Diffraction confirmed the phase purity and cubic crystal

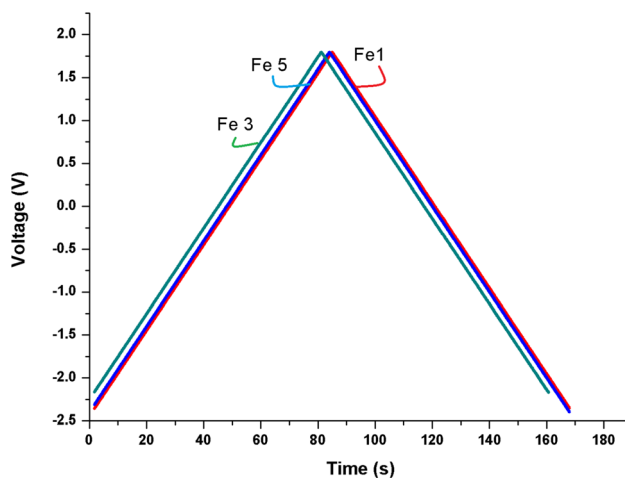
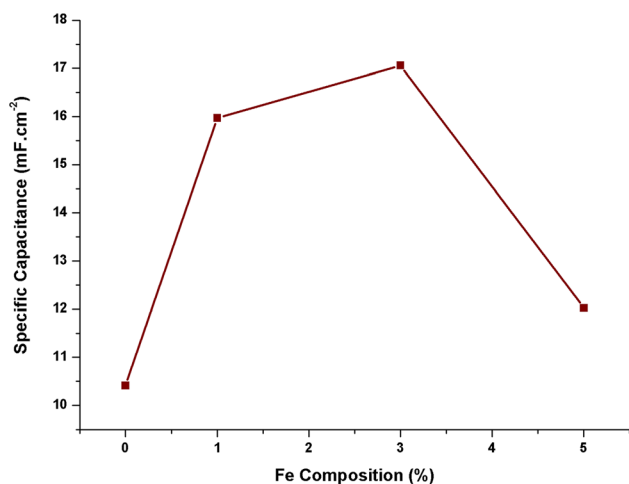


Fig. 11 Time Vs Voltage Response

Table 3 CV parameters of Fe³⁺-doped ZnS QDs

Quantum dots	Scan rate	Area	Potential window	$C_s = \frac{\text{Area}}{2 \times \text{scan rate} \times \text{Pot. window}}$
ZnS	0.1	0.17792	0.08544	10
Zn _{0.99} Fe _{0.01} S	0.1	0.17015	0.05328	15.968
Zn _{0.97} Fe _{0.03} S	0.1	0.16996	0.04981	17.058
Zn _{0.97} Fe _{0.05} S	0.1	0.23784	0.09888	12.026

**Fig. 12** Specific capacitance Vs Fe Composition

structure of the samples. The prepared QDs are sized between 1.5 and 2 nm. The TEM and SEM pictures showed the structure and morphology of the samples. The EDAX and FT-IR analyses confirmed the purity and presence of the dopant as expected for the targeted ratio. The UV-vis study suggested that the presence of Fe³⁺ ions alters the absorbance and band gap values of the samples. The absorbance peaks were slightly blue-shifted for the initial doping of Fe³⁺ ions. Highest optical transmittance received in the visible region for Fe³⁺ (5 at.%). PL-spectra blue emission peak suppression was received due to Fe³⁺ doping. A better electrochemical response was received for Fe³⁺ (5 at.%). High specific capacitance was received for 3 at.% Fe³⁺-doped ZnS QDs. The limitation of the present synthesis is tuning the particle size, achieving quantum confinement, and tailoring the band gap. The wide band gap tailoring is still possible for the future. Since the composition of Fe³⁺ doped ZnS QDs exhibited excellent optical and electrical behaviours, this composition may be suitable for optoelectronic device fabrication. An increase in the specific capacitance values of Fe³⁺-doped ZnS QDs with stability can find applications for high energy density devices.

References

- [1] Y Xu et al. *Nanoscale* **13** 8004 (2021)
- [2] W Zhou and J J Coleman *Curr. Opin. Solid State Mater. Sci.* **20** 352 (2016)
- [3] I V Martynenko, A P Litvin, F Purcell-Milton, A V Baranov, A V Fedorov and Y K Gun'ko *J. Mater. Chem. B* **5** 6701 (2017)
- [4] W W Chow and F Jahnke *Prog. Quant. Electron.* **37** 109 (2013)
- [5] J Owen and L Brus *J. Am. Chem. Soc.* **139** 10939 (2017)
- [6] O Kulakovich et al. *Nanotechnology* **32** 035204 (2021)
- [7] M Afzaal and P O'Brien *J. Mater. Chem.* **16** 1597 (2006)
- [8] M Peng, Z Wen and X Sun *Adv. Func. Mater.* **33** 2211548 (2023)
- [9] J Wang, Y Xing, F Wan, C Fu, C H Xu, F X Lianga and L B Luo *J. Mater. Chem. C* **10** 12929 (2022)
- [10] X Guo, J Wang, M Zhang and M L Fauconnier *Handbook of II-VI Semiconductor-Based Sensors and Radiation Detectors.* (ed.) G Korotcenkov (Cham: Springer) (2023)
- [11] H Qi, S Wang, X Jiang, Y Fang, A Wang, H Shen and Z Du *J. Mater. Chem. C* **8** 10160 (2020)
- [12] A Mera, Q Mahmood and S A Rouf *Solid State Commun.* **352** 114835 (2022)
- [13] N Erum and J Ahmad *Opt. Quant. Electron.* **55** 337 (2023)
- [14] X Fang, T Zhai, U K Gautam, L Li, L Wu, Y Bando and D Golberg *Prog. Mater. Sci.* **56** 175 (2011)
- [15] P D'Amico, A Calzolari, A Ruini and A Catellani *Sci. Rep.* **7** 1685 (2017)
- [16] G Gurung, T K Ekanayaka, A J Yost and T R Paudel *Mater. Res. Express* **6** 126550 (2019). <https://doi.org/10.1088/2053-1591/ab56d6>
- [17] R Abimaheshwari, P Sakthivel and S V Vijayasundaram *J. Phys.* **96** 3755 (2022)
- [18] H Lu, S-J Ho, H-S Chen and AC-M Yang *ACS Appl. Nano Mater.* **4** 2 2108–2117 (2021). <https://doi.org/10.1021/acsnm.0c03396>
- [19] K Sharma, P Kumar, G Verma and A Kumar *Optik* **206** 164357 (2020)
- [20] E Soheyli, R Sahraei and G Nabiyouni *J. Lumin.* **205** 525 (2019)
- [21] Q Wang, P Xu, G Zhang, W Zhang, L Hu and P Wang *Phys. Chem. Chem. Phys.* **20** 18601 (2018)
- [22] P Sakthivel, S Muthukumar and M Ashokkumar *J. Mater. Sci. Mater. Electron.* **26** 1533 (2015)
- [23] M S Akthar, M A Malik, Y G Alghamdi, K S Ahmed, S Riaz and S Naseem *Mater. Sci. Semicond. Process.* **39** 283 (2015)
- [24] S Jindal and P Sharma *J. Alloys Compd.* **879** 160383 (2021)
- [25] Y Li, C Cao and Z Chen *Chem. Phys. Lett.* **517** 55 (2011)
- [26] B Sreenivasulu, S V Reddy and P Swapna *J. Mater. Sci. Mater. Electron.* **31** 16150 (2020)
- [27] Q Mahmood, M Hassan and N A Noor *J. Supercond. Nov. Magn.* **30** 1463 (2017)
- [28] M D AbulMomin, M D AminulIslam and A Majumar *Int. J. Quantum Chem.* **121** e26786 (2021)

- [29] M Zeng, Y Ma, Y Wang and C Pei *Ceram. Int.* **38** 6951 (2012)
- [30] P Sakthivel, K Kavirasu, G K D PrasannaVenkatesan and A Vilorio *Spectrochim. Acta A* **241** 118666 (2020)
- [31] I Devadoss, P Sakthivel and A Krishnamoorthy *J. Mater. Sci. Mater. Electron.* **32** 5729 (2021)
- [32] V Boiko, Z Dai, M Markowska, C Leonelli, C Mortalò, F Armetta, F Ursi, G Nasillo and M L Saladino *Sci. Rep.* **11** 141 (2021)
- [33] P Kumari, K P Misra, S Samanta, A Rao, A Bandyopadhyay and S Chattopadhyay *J. Lumin.* **251** 119258 (2022)
- [34] I Devadoss and P Sakthivel *Appl. Phys. A.* **126** 315 (2020)
- [35] P Sakthivel and S Muthukumaran *Opt. Laser. Technol.* **103** 109 (2018)
- [36] K Sharm, P Kumar, G Verm and A Kumar *Optik.* **206** 164357 (2020)
- [37] B M Tissue *Charact. Mater.* (2012). <https://doi.org/10.1002/0471266965.com059.pub2>
- [38] I Devadoss, P Sakthivel and S P Sheeba *J. Phys.* **95** 741 (2021)
- [39] A Krishnamoorthy, P Sakthivel, I Devadoss and V M I Muthaiya *Optik* **205** 164220 (2020)
- [40] M Wu, Z Wei, W Zhao, X Wang and J Jiang *J. Nanomater.* **2017** 1603450 (2017)
- [41] S Kumar and N K Verma *J. Mater. Sci.* **26** 2754 (2015)
- [42] R Kumar, P Sakthivel and P Mani *Appl. Phys. A* **125** 1 (2019)
- [43] A Krishnamoorthy, P Sakthivel, I Devadoss and S N Anitha Rajathi *Appl. Sci.* **3** 694 (2021)
- [44] R E ElShater, H S El-Desoky, T M Meaz, M M Rajesh Kumar and J Abdel-Galeil *Mater. Sci. Mater. Electron.* **34** 842 (2023)

Publisher's Note Springer Nature remains neutral with regard to jurisdictional claims in published maps and institutional affiliations.

Springer Nature or its licensor (e.g. a society or other partner) holds exclusive rights to this article under a publishing agreement with the author(s) or other rightsholder(s); author self-archiving of the accepted manuscript version of this article is solely governed by the terms of such publishing agreement and applicable law.